Investigation of the [Cp*Mo(PMe 3) 3 H] n + (n = 0, 1) Redox Pair: Dynamic Processes on Very Different Time Scales

Miguel Baya, Pavel Dub, Jennifer Houghton, Jean-Claude Daran, Natalia V Belkova, Elena S. Shubina, Lina M Epstein, Agusti Lledos, Rinaldo Poli

Investigation of the $[Cp^*Mo(PMe_3)_3H]^{n+}$ (n = 0, 1) redox pair: dynamic processes on very different time scales

Miguel Baya,[a,b†] Pavel A. Dub,[a,c,d] Jennifer Houghton,[a] Jean-Claude Daran,[a,d] Natalia V. Belkova,[c] Elena S. Shubina*,[c] Lina M. Epstein,[c] Agustí Lledós*,[b] Rinaldo Poli*[a,d,e]

[a] *CNRS; LCC (Laboratoire de Chimie de Coordination); 205, route de Narbonne, F-31077 Toulouse, France; Fax: (+) 33-561553003; E-mail: poli@lcc-toulouse.fr*

[b] *Departament de Química, Edifici Cn, Universitat Autónoma de Barcelona, 08193 Bellaterra, Spain*

[c] *Nesmeyanov Institute of Organoelement Compounds, Russian Academy of Sciences, Vavilov Street 28, 119991 Moscow, Russia*

[d] *Université de Toulouse; UPS, INP; F-31077 Toulouse, France*

[e] *Institut Universitaire de France, 103, bd Saint-Michel, 75005 Paris, France*

† Present address: Departamento de Química Inorgánica, Instituto de Ciencia de Materiales de Aragón, Universidad de Zaragoza-CSIC, 50009. Zaragoza, Spain

Summary

Compound [Cp*Mo(PMe_3)$_3$H] (**1**) is reversibly oxidized at $E_{1/2}$ = -1.40 V vs. ferrocene in MeCN. Its oxidation with Cp_2FePF_6 yields thermally stable [Cp*Mo(PMe_3)$_3$H]PF_6 (**2**), which has been isolated and characterized by IR and EPR spectroscopy and by single-crystal X-ray diffraction. The ^{1}H and ^{31}P NMR spectra of **1** show two types of PMe_3 ligands in a 1:2 ratio at low temperature, but only one average signal at room temperature, with activation parameters of $\Delta H^{\ddagger}$ = 11.7(3) kcal mol^{-1} and $\Delta S^{\ddagger}$ = -3(1) e.u. for the exchange process. Although only one species is evidenced by NMR for **1** and by EPR for **2**, the solution IR spectra of each complex show two bands in the ν(Mo-H) region (**1**: major at 1794 cm^{-1} and minor at ca. 1730 cm^{-1}; **2**: ca. 1800 and 1770 cm^{-1} with approximately equal intensity), the position and relative intensity being little dependent on solvent. A thorough DFT investigation suggests that these are different rotamers involving different relative orientations of the Cp* ring and the PMe_3 ligands in these complexes. This ring rotation process is very rapid on the NMR and EPR timescale but slow on the IR timescale. The X-ray data and the theoretical calculations suggest the presence of weak Mo-H···F interactions in compound **2**. The possibility of PMe_3 dissociation, as well as other intramolecular rearrangements, for **1** and **2** is excluded by experimental and computational studies. Protonation of **1** yields [Cp*Mo(PMe_3)$_3$H$_2$]$^+$ (**3**) which also reveals a dynamic process interconverting the two inequivalent H ligands and the three PMe_3 ligands (two sets in a 1:2 ratio in the frozen structure) on the NMR timescale (activation parameters of $\Delta H^{\ddagger}$ = 9.3(1) kcal/mol and $\Delta S^{\ddagger}$ = -4.1(4) e.u.). A DFT study suggests that this exchange process occurs via a low energy symmetric dihydride intermediate and not through a dihydrogen complex.

Keywords: Molybdenum, Phosphine ligands, Cyclopentadienyl ligands, Paramagnetic hydride complex, Dihydrogen bonding, DFT calculations

Introduction

Hydride complexes generally feature a closed shell configuration. They are implicated in a variety of catalytic cycles and are also intermediates of C-H oxidative addition processes. Open-shell, paramagnetic versions, on the other hand, have not so far demonstrated broad utility, mainly because of their instability and multitude of decomposition pathways, including deprotonation,[1] disproportionation,[2] dihydrogen reductive elimination (for complexes containing at least two hydride ligands),[3] atom transfer, etc.[4] Yet, fundamental processes such as dihydrogen evolution in Nature appear to take place via open-shell hydride complexes.[5-8] It is also possible to imagine potential implication in electrocatalytic hydrocarbon oxidation. Therefore, paramagnetic hydride complexes are attracting renewed interest. It has long been known that one-electron oxidation of hydride complexes increases the M-H bond acidity.[1] However, this property highly depends on the medium.[9, 10] For instance, hydride complexes with hydridic character may be strong acids in water.[10]

Many oxidized hydride complexes spontaneously decompose by transferring a proton to a base, which may be the 18-electron hydride precursor itself.[4] Suppression of this reactivity has been achieved by the use of strong donating ligands possessing, at the same time, a significant steric bulk.[11, 12] We have previously shown that the electron-rich hydride complex $[CpMo(PMe_3)_3H]$ is reversibly oxidized to yield unstable 17-electron $[CpMo(PMe_3)_3H]^+$,[13] which decomposes by deprotonation and disproportionation at room temperature. We have therefore turned our attention to the bulkier and electron-richer Cp* analogue, $[Cp^*MoH(PMe_3)_3]$, **1**.[14] In this contribution, we will show that this is indeed leading to a more stable one-electron oxidation product, $[Cp^*MoH(PMe_3)_3]^+$, **2**. We present here the synthesis and characterization of this material, including detailed spectroscopic studies, and a computational investigation designed to elucidate the nature of a second product that has been detected in solution for both **1** and **2**.

Results and Discussion

(a) Synthesis and characterization of $[Cp^*Mo(PMe_3)_3H]^+PF_6^-$, 2.

A cyclic voltammetric study of **1** shows a reversible oxidation process (ΔE_p = 64 mV; *cf.* 67 mV for ferrocene under the same conditions) at $E_{1/2}$ = -1.40 V *vs.* ferrocene in MeCN (-1.35 V in THF). This should be compared with the reversible oxidation of the analogous Cp compound at $E_{1/2}$ = -1.46 V *vs.* ferrocene in MeCN. These low potentials make these complexes stronger reductant than Cp_2Co (for which $E_{1/2}$ = -1.33 V *vs.* ferrocene in CH_2Cl_2), although not as strong as Cp^*_2Co ($E_{1/2}$ = -1.94 V).[15] We are not aware of other hydride complexes with such low $E_{1/2}$ values. Note that the oxidation of **1** is slightly less facile than that of the Cp analogue. This is an unexpected result, because replacement of Cp with the electron-richer Cp* ligand usually causes a considerable negative shift in the oxidation potential. The reason of this trend reversal is unclear and is still under investigation. In line with our expectations (see Introduction), however, the 1-electron oxidation product **2**, generated by oxidation of $[Cp^*Mo(PMe_3)_3H]$ with 1 equiv. of Cp_2FePF_6 in THF (see equation 1), is thermally more stable than the Cp analogue. It is moderately stable in MeCN at room temperature, decomposing slowly over a period of 24 h and could be crystallized by slow diffusion of either diethyl ether or pentane into a THF solution at –40°C to yield suitable single crystals for an X-ray analysis. In the solid state, the compound does not significantly deteriorate upon standing in air at room temperature, in contrast to the extreme air sensitivity of its precursor **1**. A view of the molecule is shown in Figure 1. Relevant bonding parameters are collected in Table 1. The coordination geometry around the Mo atom is that of a typical 4-legged piano stool. The hydride H atom was directly located from difference Fourier maps and freely refined. Although the Mo-H distance of 1.72(6) Å is not very accurately determined, it corresponds closely to the Mo-H distances determined by neutron diffraction

for other Mo hydride compounds: 1.685(3) Å for Cp_2MoH_2,[16] 1.69(5) Å for Mo(H)(η^2-Me_2C=NAr)[N*i*Pr(3,5-$C_6H_3Me_2$)]$_2$,[17] 1.712(8), 1.719(9) and 1.719(9) Å for (1,2,4-C_5H_2*i*Bu_3)Mo(PMe_3)$_2H_3$,[12] and 1.789(7) for Cp*Mo$(CO)_3$H.[18]

$$[Cp^*Mo(PMe_3)_3H] + Cp_2FePF_6 \rightarrow Cp_2Fe + [Cp^*Mo(PMe_3)_3H]^+PF_6^- \qquad (1)$$

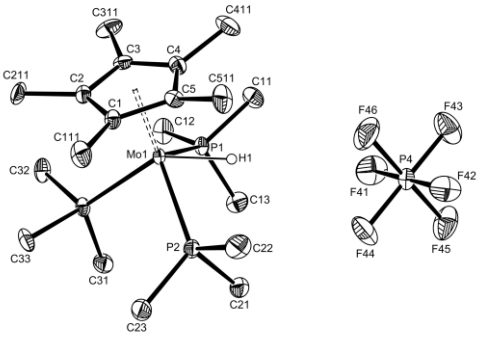

Figure 1. An ORTEP view of compound **2** (ellipsoids are drawn at the 30 % probability level). All hydrogen atoms except the hydride are not shown for clarity.

One interesting structural feature is the relative location of the two ions, with the PF_6^- ion facing the cation on the same side as the hydride ligand. Since the oxidation of hydride complexes is known to often induce decomposition by deprotonation,[4] this observation suggests that the hydride ligand has become polarized δ+ and that it establishes a Coulombic interaction with the PF_6^- anion. The H···F distances are quite long (3.33, 3.56 and 3.58 Å) for consideration as hydrogen bonds, but the PF_6^- ion is prevented from more closely approaching the hydride ligand by contacts with a number of Cp* and PMe_3 H atoms (see Figure S1 in the Supporting Information; the shortest contacts being F41···H11A, 2.80; F44···H21D, 2.50; F46···H51A, 2.85 Å). For other previously described cationic paramagnetic hydride complexes, for instance $[Cp^*W(dppe)H_3]^+PF_6^-$,[3] $[(1,2,4\text{-}C_5H_2t\text{Bu}_3)Mo(PMe_3)_2H_3]^+PF_6^-$,[11] and $[(1,2,4\text{-}C_5H_2t\text{Bu}_3)Mo(PMe_3)_2H]^+PF_6^-$,[11] no significant contacts were observed between the

anion and the hydride ligand(s). The question of the charge on the hydride ligand in this compound has been addressed by computational methods (*vide infra*).

Table 1. Selected bond distances (Å) and angles (°) for compound **2** and comparison with the DFT-optimized parameters for the cation in the gas phase.[a]

	Experimental (X-ray)	DFT-optimized (cation)	DFT-optimized (cation+anion)
CNT-Mo	2.0021(6)	2.067	2.071
Mo-H	1.72(6)	1.699	1.691
Mo-P_t	2.490(2)	2.598	2.565
Mo-P_c	2.480(2)	2.553	2.551
Mo-P_c	2.475(2)	2.555	2.563
CNT-Mo-H	107(2)	105.91	106.23
CNT-Mo-P_t	114.66(5)	116.56	116.21
CNT-Mo-P_c	122.34(5)	121.16	123.26
CNT-Mo-P_c	121.97(6)	120.76	120.13
H-Mo-P_t	138(2)	137.45	137.55
H-Mo-P_c	70(2)	69.60	66.70
H-Mo-P_c	66(2)	67.43	67.82
P_t-Mo-P_c	88.94(7)	89.76	89.64
P_t-Mo-P_c	89.20(7)	87.86	89.43
P_c-Mo-P_c	109.33(7)	111.17	108.85

[a]The subscripts in P_c and P_t refer to the position *cisoid* and *transoid* to the hydride ligand.

In agreement with the presence of a single unpaired electron, solutions of complex $[Cp^*Mo(PMe_3)_3H]^+$ in THF are EPR active. However, the isotropic spectrum is rather broad (width = 274 G at 273 K) and does not reveal any hyperfine structure, in contrast to the sharp EPR spectrum of the Cp analogue.[13] Cooling the sample does not result in any significant sharpening down to the freezing point. A frozen glass spectrum exhibits an essentially cubic tensor and is much sharper (width = 21.3 G at 110K) than the isotropic spectrum, but insufficiently so to reveal any hyperfine coupling. Figures of these spectra are available as supporting information (Figure S2 and S3). Whereas the neutral precursor is unstable in CH_2Cl_2 solution, leading to hydride transfer to the solvent and formation of

$Cp^*Mo(PMe_3)_3Cl$,[19] the oxidized complex is stable under the same conditions. This is in line with the expected hydridicity reduction upon oxidation.

(b) Infrared characterization of complexes 1 and 2.

The ground state properties of the Mo-H bond for the neutral and cationic complexes were probed by infrared spectroscopy in solution (Figure 2). An immediately striking observation is the presence of two bands in each case, whereas only one band is expected for a monohydride complex. A major band around 1794 cm^{-1} and a minor one at ca. 1730 cm^{-1} are observed in both *n*-hexane and THF for **1**, whereas two bands of approximately equal intensity at ca. 1800 and 1770 cm^{-1} are observed in both THF and CH_2Cl_2 for the cationic complex **2**. The observed blue shift upon oxidation parallels that reported for other redox couples, for instance $[CpFeH(dippe)]^{0/+\bullet}$ ($\Delta\nu_{M\text{-}H}$ = +28 cm^{-1}) and $[Cp^*FeH(dippe)]^{0/+\bullet}$ ($\Delta\nu_{M\text{-}H}$ = +14 cm^{-1}).[20] The parallel magnetic resonance investigations (NMR for **1** and EPR for **2**) did not show any evidence for the presence of more than one species in solution. However, the timescale of the magnetic resonance techniques is longer than that of infrared spectroscopy, thus they may reveal average resonances of rapidly equilibrating species. The alternative possibility that the second band is due to a Fermi resonance appears discarded, at least for compound **1**, by the observation that both bands disappear upon carrying out an H/D exchange at the hydride position. The exchange was quite slow in CD_3OD at room temperature, since the two bands decreased only by a factor of ca. 50% upon stirring overnight, but both decreased by essentially the same factor (I_{major}/I_{minor} = 2.89 initially, 2.57 after overnight stirring and 47% conversion) proving that they belong to two difference hydride species in rapid equilibrium. The corresponding Mo-D stretching vibrations (expected at *ca.* 1270-1220 cm^{-1}) could not be observed because of their very low relative intensity and because many other bands are present in this region of the spectrum. However, positive evidence for the formation of $[Cp^*Mo(PMe_3)_3D]$ was obtained by ^{2}H-NMR, with the

observation of a quartet resonance at δ -5.23 ($^2J_{DP}$ = 7.4 Hz) in ca. 30:70 C_6D_6-CD_3OD (*cf.* δ -4.88 with $^2J_{HP}$ = 47.5 Hz in the ^1H NMR under the same conditions).

Contrary to the solution infrared spectra, the solid state spectra of **1** and **2** do not clearly reveal a second component. In the spectrum of **1** (Figure 2(a)), the presence of a second low-frequency component is not completely excluded because of the large band width (the band marked with an asterisk centered at 1650 cm^{-1} results from decomposition, as shown by its irreproducible intensity from different samples and time evolution, due to the extreme air sensitivity of **1**), but the spectrum of **2** (Figure 2(b)) quite clearly shows the presence of a single component centered at 1786 cm^{-1}. Note that the asymmetric unit in the crystal structure of **2** contains only one molecule (one cation and one anion). For both compounds, the band observed in the solid state is closest to the higher frequency band observed in solution.

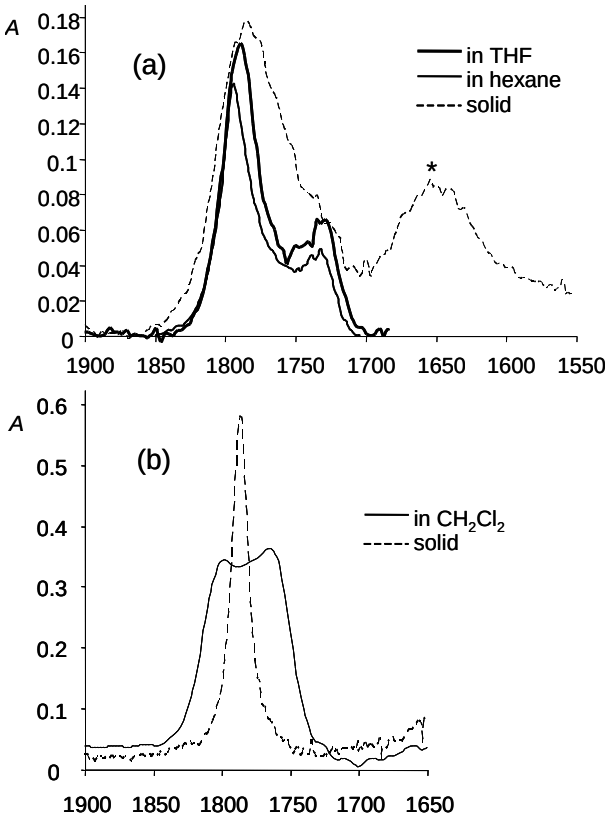

Figure 2. Infrared spectra of: (a) complex $Cp^*Mo(PMe_3)_3H$ (0.08 M, 0.4 mm pathlength) at room temperature (thinner line: in hexane; thicker line: in THF); (b) complex $[Cp^*Mo(PMe_3)_3H]PF_6$ (0.042 M, 1.2 mm pathlength) in CH_2Cl_2 at 200 K. The band labelled with an asterisk in Figure 2a is due to an oxidation impurity (see text).

The two bands have a smaller intensity difference in **2**. Under the assumption of similar extinction coefficients for the Mo-H vibration in the two species, this means that the two species are more equally populated (smaller free energy difference) in **2**. The solution IR spectra recorded at different temperatures (supporting Figures S4 and S5) showed a change of the band intensity ratio, this being more evident for **1** where the Boltzmann population difference is greater. For the neutral complex, an estimation of ca. 0.2 kcal/mol as ΔG (G_{minor}-G_{major}) can be derived from the I(1800)/I(1730) ratios at the two extreme temperatures: 2.95 at 290 K and 3.5 at 200 K.

The two possibilities envisaged for such equilibrating species are (*i*) a phosphine ligand dissociation and (*ii*) a geometric isomerism. In order to probe for the ligand dissociation hypothesis, spectroscopic studies were carried out in the presence of deliberately added PMe_3. The measurement of the intensity ratio of the two IR bands (conditions as in Figure 2, with 10 equiv of PMe_3) was prevented by the strong absorption of free PMe_3 in the Mo-H stretching region. Useful information, however, could be obtained by NMR and EPR spectroscopy. For the neutral complex, the ^{1}H and ^{31}P NMR spectra of **1**/PMe_3 mixtures showed the superposition of the distinct free ligand and hydride complex resonances, demonstrating that ligand exchange between coordinated and free PMe_3 is slow in the NMR timescale. Together with the absence of the ^{1}H and ^{31}P NMR resonances of free PMe_3 for a solution of pure **1**, this observation rules out the presence of a dissociation equilibrium. Concerning the **2**/PMe_3 solutions, the ^{1}H and ^{31}P NMR spectra showed sharp resonances at the usual diamagnetic position for the free PMe_3, unaffected by the presence of the paramagnetic complex. Thus, ligand exchange is slow on the NMR timescale also for the cationic complex. The parallel EPR investigation shows that the presence of free PMe_3 does not alter the linewidth of the observed resonance. Therefore, no significant PMe_3 dissociation is suggested. Hence, we

remain with the option of a dynamic process interconverting two different stereoisomers. This possibility was addressed in more detail by DFT calculations (see section d below).

(c) Low-temperature NMR study of compound 1.

Compound **1** has already been described,[14, 21] but its NMR investigation was limited to room temperature, showing a single ^{31}P resonance and a binomial quartet ^{1}H resonance for the hydride signal. This shows that either the three PMe_3 ligands occupy symmetry-equivalent positions or that a rapid dynamic exchange process is occurring. The peculiar IR spectrum observed for compound **1** has encouraged us to carry out a new NMR investigation at variable temperatures.

The shape of the hydride resonance in the ^{1}H NMR spectrum changes upon cooling to ultimately yield a doublet of triplets (Figure 3), demonstrating the presence of a dynamic behaviour and two types of inequivalent PMe_3 ligands (in a 2:1 ratio) in the ground state structure. The hydride nucleus has a stronger coupling (J = 77 Hz) with the two equivalent P nuclei and a smaller one (J = 13 Hz) with the unique P nucleus. The two different types of P nuclei are coupled to each other in the low-T $^{31}P\{^{1}H\}$ spectrum with a J of 54 Hz. Simulations with SpinWorks[22] provided an excellent fit, at each temperature, of both ^{1}H and $^{31}P\{^{1}H\}$ spectra with the same mutual exchange rate constant (data in the Supporting Information). The Eyring analysis of the temperature dependent rate constants provided the activation parameters for the mutual exchange: $\Delta H^{\ddagger}$ = 11.7(3) kcal mol^{-1}; $\Delta S^{\ddagger}$ = -3(1) e.u. The most obvious structure of **1** that fits these data is the four-legged piano stool, identical to that observed by X-ray diffraction for the corresponding cation **2**. We were not successful in growing single crystals of compound **1**, but assuming that the geometry, particularly the bond angles, is not significantly different than that observed for **2**, it is interesting to note that the pseudo-*trans* P nucleus shows the weaker coupling and the pseudo-*cis* P nuclei the stronger one, contrary to the typical situation for *trans* and *cis* arrangements in square planar and

octahedral complexes. Stronger coupling in four-legged piano stool geometries between pseudo-*cis* ligands relative to pseudo-*trans* ligands have also been observed in other compounds, notably $CpMo(CO)_2(PR_3)H$ (R = Me, Ph, Cy)[23-25] and $CpOs(PiPr_3)H_3$.[26]

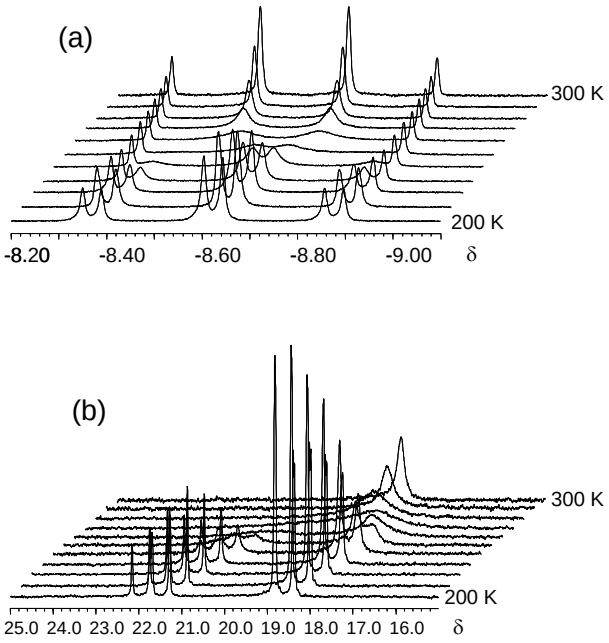

Figure 3. Variable temperature ^1H (a) and $^{31}P\{^1H\}$ (b) NMR properties of compound $Cp^*Mo(PMe_3)_3H$ in toluene-d_8. Spectra were taken at 10 K intervals, between 200 and 300 K.

The most interesting observation is the *absence* of any other hydride resonance in the low-temperature spectra. According to the low-temperature IR study (*vide supra*) a significant amount of the minor isomer (20%) remains present at 200 K, under the assumption that the extinction coefficient for the Mo-H vibration is the same in both species. Since no separate NMR resonance is observed for this isomer, we conclude that the dynamic process that exchanges the major and minor species observed in the IR spectrum is faster than the dynamic process that exchanges the inequivalent PMe_3 ligands in the ground state structure. Furthermore, this dynamic process must maintain the chemical inequivalence of the PMe_3 ligands.

The PMe_3 exchange process must take place through a more symmetric, higher energy intermediate or transition state. In the case of an intermediate, this is not significantly populated in the temperature range used in our study and is therefore unobserved by IR spectroscopy. The most likely candidate is a pseudo-trigonal bipyramidal structure, characterized by *trans* Cp* and H ligands in the axial positions and equivalent PMe_3 ligands in the pseudo-trigonal plane. As will be shown later in the DFT section, a higher energy local minimum is indeed observed for this geometry. Examples of pseudo-trigonal bipyramidal structures for $CpML_4$ complexes are known,[27, 28] and the interconversion mechanism between these two geometries has been addressed.[29]

In conclusion, the combined IR and NMR investigation of compound $[Cp^*Mo(PMe_3)_3H]$ demonstrates that there must be at least three structures in solution: the ground state structure with inequivalent PMe_3 ligands in a 2:1 ratio (presumably a 4-legged piano stool), a symmetric intermediate responsible for the mutual PMe_3 exchange process (presumably a trigonal bipyramid) that is not thermally populated, and a second asymmetric, thermally populated structure (at ca. 0.2 kcal/mol in enthalpy from the ground state) that exchanges rapidly with the ground state structure on the NMR time scale, but not on the IR time scale. The nature of these structures has been explored by the DFT calculations.

(d) DFT study of the ground state structures of 1 and 2 and exchange barriers

Geometry optimizations were run for both neutral and cationic complexes, using systems $[(C_5R_5)Mo(PR'_3)_3H]^{n+}$ (n = 0, 1), with R = R' = H (**A**), R = H, R' = Me (**B**), and R = R' = Me (**C**, real systems). All optimized geometries, as well as tables of optimized distances and angles, Mo-H stretching frequencies, and a discussion of the structural changes as a function of the chosen model (**A**, **B** or **C**), are provided as supporting information.

The most stable structure was in all cases the typical 4-legged piano stool (**PS**), independent of the model and of the oxidation state. This agrees with our assignment of the

observed major ν(Mo-H) band of **1** to the **PS** isomer. The calculated Mo-H stretching frequencies of **1C-PS** and **2C-PS** (1794 and 1836 cm^{-1} respectively) qualitatively reproduce the experimental trend of a blue shift upon oxidation. The optimized distances and angles for **2C-PS** compare quite well with those experimentally determined by X-ray diffraction (see Table 1), attesting to the suitable level of theory used for the calculations. Comparison of the optimized structures of each redox pair shows interesting trends. The Mo-P distances are longer (by 0.06 - 0.15 Å) for the oxidized species, whereas the Mo-CNT (ring centroid) and Mo-H distances show a smaller dependence on the metal oxidation state, which is generally in the opposite direction (shorter in the higher oxidation state). These trends cannot be verified experimentally in the absence of an X-ray structure of compound **1**, but were noted recently in the related pair of structurally characterized $[(\eta^5\text{-}1,2,4\text{-}C_5H_2tBu_3)Mo(PMe_3)_2H_3]^{n+}$ (n = 0, 1) complexes.[12]

Calculations were also run for the ion pair, $[Cp^*Mo(PMe_3)_3H]^+PF_6^-$, in the gas phase, in order to probe the nature of the cation-anion interaction. The optimized geometric parameters are shown in Table 1. The geometry of the cation is relatively close to that calculated for the isolated cation. The optimization was conducted starting from the relative cation-anion orientation as found in the crystal structure, but the PF_6 anion rearranges itself during the optimization procedure to yield two shorter contacts with the hydride ion (Figure 4). These are significantly shorter than in the crystal, suggesting the presence of an attractive force between the hydride ligand and the fluorine atoms of the PF_6^- ion. Indeed, the Mulliken charge calculated for the hydride ligand in **2** is slightly positive (+0.017), whereas it is negative in **1** (-0.106) and also, although to a lesser extent, in the isolated cation of **2** (-0.066). This Mulliken charge changes confirm the effect of oxidation on the metal-hydride bond polarization and underline the importance of the cation-anion interaction for this polarization. In further support of an attractive force between the hydride ligand and the PF_6^- ion, the related optimization of the adduct of PF_6^- and diamagnetic **1** features much longer H···F

separations (2.819, 3.210 and 3.375 Å). The experimentally observed H···F separations in **2** are much longer than the optimized values, possibly because of the effect of neighboring pairs (crystal packing), or because the computational method overestimates the strength of these interactions.

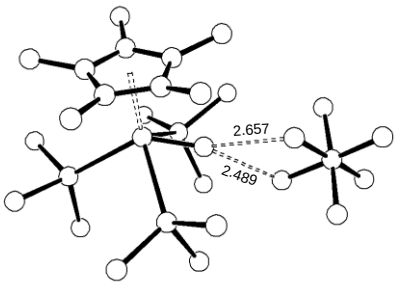

Figure 4. Gas-phase optimized geometry of $[Cp^*Mo(PMe_3)_3H]PF_6$. Hydrogen atoms on the Cp* and PMe_3 ligands have been omitted for clarity.

Energy minima corresponding to a pseudo-trigonal bipyramidal geometry (**TBP**), with the hydride and cyclopentadienyl ligands occupying the apical positions, were also located for all model systems in both oxidation states. The geometry with an apical phosphine ligand is unstable and collapses back to the lower energy minimum. We have also optimized the transition state (**TS**) leading from the ground state **PS** geometry to the **TBP** intermediate. The energies for all models, relative to those of the corresponding **PS** isomer, are visually summarized in Figure 5. Note that the relative energy for **1C-TS** is consistent with the experimentally observed barrier for the mutual PMe_3 exchange process ($\Delta H^{\ddagger}$ = 11.7(3) kcal mol^{-1}).

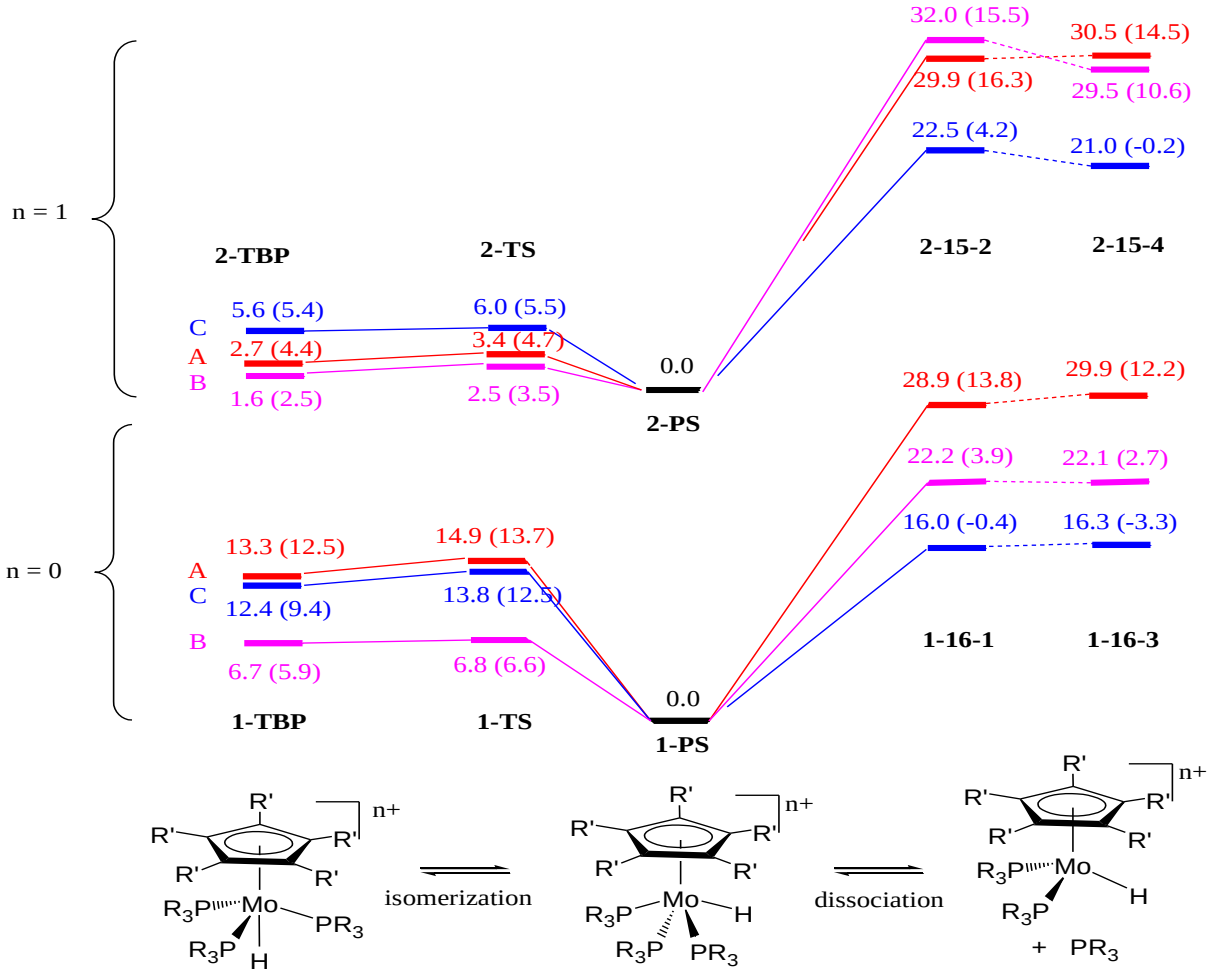

Figure 5. Relative energies and gas-phase free energies (in parentheses), in kcal mol^{-1}, for the isomerization and phosphine dissociation process for models of Cp*Mo(PMe$_3$)$_3$H (below) and its one-electron oxidation product (above). The energy values are used to represent the states on the vertical scale. For the definition of the labels (**A**, **B**, **C**, **1**, **2**, **TBP**, **TS**, **16-1**, **16-3**, **15-2** and **15-4**, see text).

In search for a third isomer for **1** and **2**, the energy of which is closer to that of the **PS** isomer, we have considered the following possibilities: a second minimum along the Berry pseudo-rotation coordinate (**BPR**), an agostic cyclopentadiene derivative (**AC**), a σ-complex with a C-H bond of a dissociated phosphine ligand (**AP**), and a Cp rotamer (**ROT**), as illustrated in Scheme 1. A different minimum in the Berry pseudo-rotation pathway might be allowed by the presence of two competitive preferred distortions of the ideal **PS** geometry.[30, 31] The **AC** geometry has previously been proposed and optimized for an intermediate of the isomerization process of the isoelectronic [Cp*Fe(dppe)H$_2$]$^+$ complex.[32] The **AP** geometry,

where the dissociated PMe_3 ligand must necessarily be *transoid* to the hydride in order to maintain the P inequivalence in the low-temperature NMR, may be made energetically favourable by the metal electron richness. Finally, two distinct minima around the Mo-Cp* axis are justified by the symmetry mismatch of the Cp* ring (five fold) and ML_4 moiety (pseudo four fold).

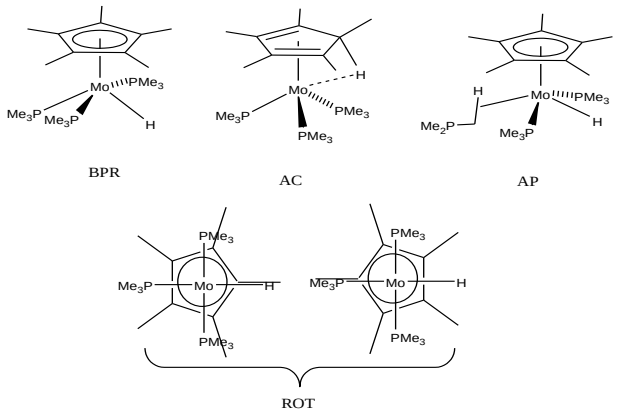

Scheme 1

The calculations on the **BPR**, **AC** and **AP** hypotheses show that these cannot rationalize the experimental observation, because either no second minimum could be found or this occurred at a prohibitively high energy (details in the Supporting Information). The hypothesis of a Cp* rotamer, on the other hand, is supported by the computational results. These calculations were carried out only on the full molecule (**C** model). A scan of the energy as a function of the rotation angle is illustrated in Figure 6. The calculations show two minima around the C-CNT-Mo-H dihedral angle, with the second rotamer being located 0.56 kcal mol^{-1} higher in energy (3.08 kcal mol^{-1} in free energy) for **1C-ROT** and 0.36 kcal mol^{-1} higher in energy (but 0.04 kcal mol^{-1} *lower* in free energy) for **2C-ROT**. The highest energy corresponds, for both **1C** and **2C**, to the eclipsed geometry (C-CNT-Mo-H dihedral angle around zero). Note that the calculations reproduce, at least at a qualitative level, the lower energy difference for the two conformers in the cationic complex.

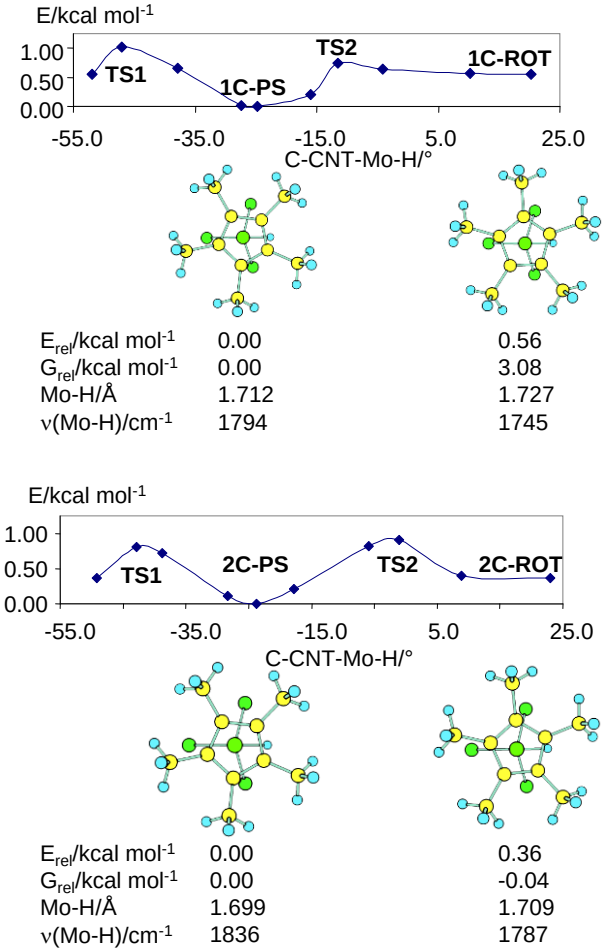

Figure 6. Energy of molecules **1C** and **2C** as a function of the C-CNT-Mo-H dihedral angle. Views of the optimized minima emphasizing the Cp* dihedral angle (the PMe_3 methyl groups have been removed for clarity) and their calculated Mo-H distances, Mo-H vibrational frequencies, and relative energies and free energies, are also shown.

The calculated Mo-H distances and vibrational frequencies are also reported in Figure 6. Notably, the calculated ν(Mo-H) of the global minimum of **1C-PS** is at higher frequency than that of the higher energy minimum, in agreement with the experiment. The calculated frequencies (1794 and 1745 cm^{-1}) are also in excellent agreement with the experimental values (1794 and 1730 cm^{-1}). For system **2C-PS**, the calculated frequencies of the nearly isoenergetic rotamers (1836 and 1787 cm^{-1}) also compare rather well with the experimentally observed ones (ca. 1800 and 1770 cm^{-1}), being blue shifted relative to the frequencies of the neutral species.

Once likely candidates for the observed species have been found, validation of their independent observation by the IR spectroscopic technique is necessary. First of all, the calculated rotational barriers shown in Figure 6 are much too low for the individual observation of the rotamers by NMR spectrometry (for the diamagnetic compound **1**). More typical barriers for processes that can be frozen on the NMR timescale are in the order of 10 kcal mol^{-1}, as found above for the P exchange process in **1**. The EPR spectroscopic technique operates on a faster timescale than NMR and fluxional processes with lower activation barriers have been investigated,[33, 34] including a substituted cyclopentadienyl ring rotation in compound $(C_5Ph_4H)Mo(CO)_2(L_2)$ (L_2 = 2,3-bis(diphenylphosphino)maleic anhydride) ($\Delta H^{\ddagger}$ = 2.2 kcal mol^{-1}).[35] However, the broadness of the EPR resonance of **2** does not permit to reveal any coalescence phenomenon. Thus, the energy profiles shown in Figure 6 are entirely consistent with the observation of only one species in solution for both **1** and **2** even at low temperatures.

Concerning the IR experiments, in order to observe separate bands for exchanging species with a frequency difference of ca. 60 cm^{-1} (as observed in **1**) or ca. 30 cm^{-1} (as observed in **2**), the exchange rate must be slower than $1.8 \cdot 10^{12}$ s^{-1} or $9 \cdot 10^{11}$ s^{-1}, respectively, corresponding to activation barriers above 0.7 or 1.1 kcal mol^{-1} according to the Eyring equation. The calculated free energy barriers for the Cp* ring rotation (Figure 6) are indeed higher than these values (3.3 kcal mol^{-1} for **1C** and 1.51 kcal mol^{-1} for **2C**). The smaller frequency difference and the smaller calculated activation barrier for the two rotamers of **2** suggests that the spectrum of this compound is closer to the coalescence region. However, warming up this sample to 350 K in dichloroethane shows no clear evidence for the beginning of a coalescence phenomenon (Figure S5). It should be recalled that the coalescence of IR bands caused by molecular dynamics, though not as familiar as the same phenomenon in NMR spectroscopy, is well established and appreciated.[36-41]

The separate observation of different rotamers for these two redox-related compounds is worth a brief discussion because it is unusual. This is apparently the first reported case of the simultaneous IR observation of metal-hydrogen stretching vibrations in different rotamers of a cyclopentadienyl hydride complex. We attribute this observation to the concurrence of a few favourable circumstances. The first one is the highly crowded nature of the molecule, with the PMe_3 and Cp* methyl groups imposing relatively large barriers to go past each other through the Cp* ring rotation. The second one is the relatively high frequency difference for the two rotamers, created by a sufficiently different transmission of electronic and steric effects from the Cp* conformation to the Mo-H bond in the two separate minima. In addition to the above factors, we point out that metal-hydrogen stretching vibrations typically have relatively low extinction coefficients, requiring high concentrations (thus high solubility) and long optical paths for measurement of the absorption bands at reasonably high signal/noise ratio. Thus, this phenomenon may have been missed in previously investigated complexes of this type. Other hydride complexes containing the Cp* ring that have been investigated in our laboratories, for instance Cp*M(dppe)H (M = Fe,[42] Ru,[43] Os[44]) for which high quality (high S/N) spectra were obtained, only show a single band, either because there is only a single minimum around the M-Cp* rotational coordinate, or because the different minima are related by a lower rotational barrier, or because the two structures have much closer vibrational frequencies.

Even though the experimental evidence is against the occurrence of PMe_3 dissociation, the bis-phosphine complexes resulting from the dissociation of one phosphine ligand were also optimized. These are open-shell systems and may adopt two different spin states[45] (singlet and triplet for the 16-electron neutral system, doublet and quartet for the 15-electron cationic one). They will be described by codes **16-1**, **16-3**, **15-2** and **15-4**, respectively. The relative energies for each system are also shown in Figure 5. Strictly on the basis of energy, the phosphine dissociation is less favourable than isomerization to the **TBP** structure for both

oxidation state levels. If we keep into account the entropic contribution, the phosphine dissociation process becomes less disfavoured and indeed becomes the preferred process in the gas phase. However, the free energy lowering caused by the entropic contribution in a condensed phase cannot be precisely estimated, because of the partial quenching of the translational and rotational degrees of freedom.

Note that, independent on the model used for the calculation and contrary to the isomerization to **TBP**, ligand dissociation is more favourable for the neutral system. It should be noted that the phosphine bond dissociation energy is more strongly dependent on the steric bulk than on the oxidation state: it is lowered by 10 kcal mol^{-1} on going from system **A** to system **C** for **1** and by 15 kcal mol^{-1} for **2**, but only by ca. 5 kcal mol^{-1} on going from **1C** to **2C**. Therefore, phosphine dissociation becomes possible for bulkier systems. In this respect, we point out our recent isolation and crystallographic characterization of a salt of $[(1,2,4\text{-}C_5H_2tBu_3)MoH(PMe_3)_2]^+$, though this was obtained by another route (H_2 reductive elimination from $[(1,2,4\text{-}C_5H_2tBu_3)MoH_3(PMe_3)_2]^+$).[11, 12] Another point of interest is the relatively similar energy for the two possible spin configurations for the dissociation product, both for the neutral and for the cationic systems, independent on the chosen model, the difference being less than 3 kcal mol^{-1}. Given the empirical and imprecise handling of electron pairing by density functional methods,[46-50] it is not possible to make reliable predictions as to the spin state adopted by these unsaturated species. The above mentioned cationic 15-electron system containing the bulkier ($1,2,4\text{-}C_5H_2tBu_3$) ligand was found to adopt a spin quartet ground state.[11, 12]

(e) Protonation of $[Cp^*Mo(PMe_3)_3H]$

Protonation of compound **1** with HBF_4 in THF affords the cationic dihydride complex $[Cp^*Mo(PMe_3)_3H_2]^+$, **3** (equation 2). An IR study shows that both ν_{MoH} bands of **1** disappear, to give rise to only one new high frequency band at 1818 cm^{-1} (Figure 7).

$$[Cp^*Mo(PMe_3)_3H] + HBF_4 \rightarrow [Cp^*Mo(PMe_3)_3H_2]^+BF_4^- \quad (2)$$

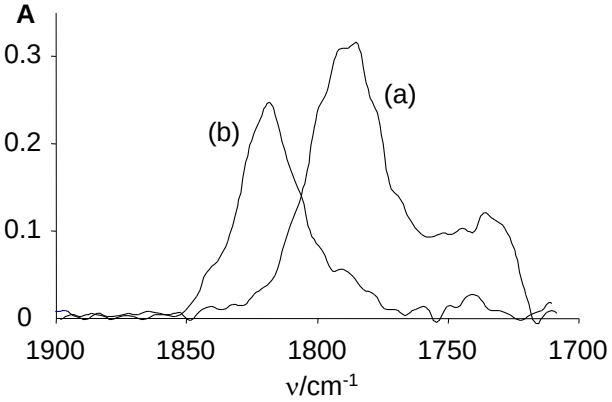

Figure 7. Change of the IR spectrum upon protonation in THF at 200 K. (*a*) $Cp^*Mo(PMe_3)_3H$. (*b*) $Cp^*Mo(PMe_3)_3H$ in the presence of 1 equiv HBF_4.

The classical nature of **3** was confirmed by the VT NMR measurements (Figure 8). At 200 K in CD_2Cl_2, the complex exhibits two separate ^1H resonances in the hydride region with a 1:1 integral ratio (doublet of triplets of small doublets at δ –3.03 and triplet of small doublets at δ –6.53) with T_1 (200 K, 500 MHz) of 280 and 330 ms, respectively. The phosphorus atoms in this complex are also non-equivalent at 200 K and appear in the $^{31}P\{^1H\}$ spectrum as a doublet and a triplet at δ 7.6 and -1.2 (J_{PP} = 23 Hz) with 2:1 integral ratio. The coupling pattern for the hydride signals was established by a series of $^1H\{sel.\ ^{31}P\}$ experiments, as shown in Figure 8. Thus, the two hydrides are coupled to each other with J_{HH} = 7 Hz. The hydride at δ -3.30 shows a stronger coupling (J_{HP} = 65 Hz) to the two equivalent P nuclei (^{31}P resonance at δ 7.6) and a weaker one (J_{HP} = 41 Hz) to the unique P nucleus (^{31}P resonance at δ -1.2). On the other hand, the hydride at δ -6.53 is significantly coupled only to the two equivalent P nuclei (J_{HP} = 45 Hz), whereas the coupling to the unique P nucleus is not clearly discernible in the $^1H\{sel.\ ^{31}P: 7.6\}$ spectrum and is estimated as ca. 10 Hz. These data are in agreement with a pseudo-octahedral geometry for **3** in which one of the hydride ligands is *trans* to Cp* ring, but do not allow to unambiguously tell which resonance belongs to

which hydride ligand. However, a comparison of the observed coupling constants of **3** with those found for **1** (where the assignment is unambiguous) and considering the similarity of the bond angles in the optimized structures of the two compounds (*vide infra* for compound **3**), strongly suggests that the signal at δ -3.30 should correspond to the axial hydride ligand and that at -6.53 to the equatorial one. A similar structure was reported for the isoelectronic $[CpW(CO)_2(PMe_3)(H)_2]^+[OTf]^-$ compound[51] and later proposed for the related $[CpMoH_2(CO)(dppe)]^+[OTf]^-$ compound.[52] It has also been observed for the isoelectronic molybdenum complex $[CpMo(PMe_3)_3(MeCN)H]^{2+}$ in its BF_4^- salt, where the pseudo-equatorial hydride position is replaced by the neutral MeCN molecule.[13]

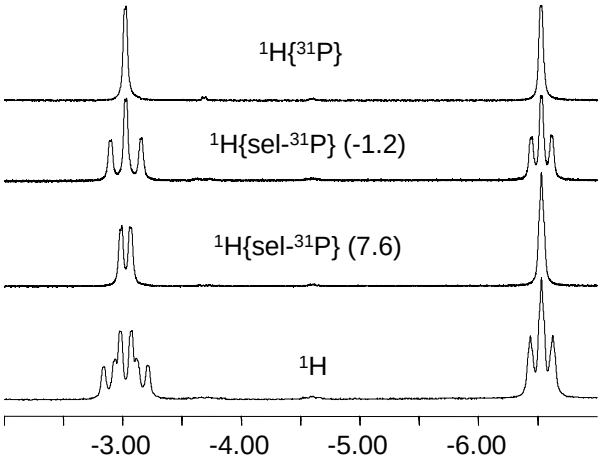

Figure 8. Low temperature (200 K) ^1H NMR spectra of compound **3** in CD_2Cl_2 with various P decoupling modes.

The ^1H hydride resonance and the ^{31}P resonances broaden with the loss of observable coupling upon temperature increase, showing coalescence at ca. 250 K. Knowledge of the full coupling pattern allowed simulation (Figure 9) and an Eyring analysis of the rate constant for the exchange process (supplemental figure S8). The rate constants for the H and P exchange processes that best fit the experimental data are essentially identical at each temperature, suggesting that the same pathway simultaneously exchanges the two types of nuclei. A least-squares Eyring fit to the data yields $\Delta H^{\ddagger} = 9.3 \pm 0.1$ kcal/mol and $\Delta S^{\ddagger} = -4.1 \pm$

0.4 e.u. for the hydride exchange process and $\Delta H^{\ddagger}$ = 9.2 ± 0.1 kcal/mol and $\Delta S^{\ddagger}$ = -4.9 ± 0.5 e.u for the P exchange process.

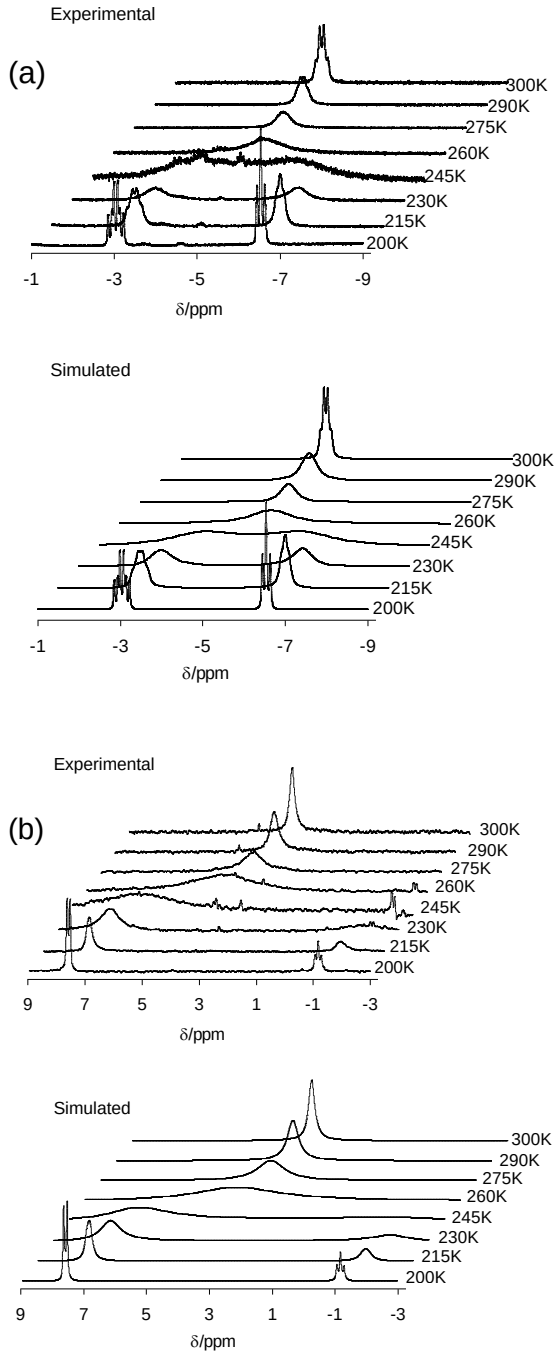

Figure 9. Experimental and simulated NMR spectra for compound **3** at various temperatures. (a) ^{1}H NMR. (b) $^{31}P\{^{1}H\}$ NMR.

(f) DFT study of compound 3

Compound **3** has also been subjected to a computational study, with the specific aim to support the proposed ground state geometry and to identify the likely hydride and phosphine exchange pathway. These calculations were carried out for the full system, $[Cp^*Mo(PMe_3)_3H_2]^+$. The results are shown in Figure 10. Three different local minima were found. The global minimum (**3a**) corresponds indeed to the asymmetric pseudo-octahedral structure, with one pseudo axial (*trans* to Cp) and one pseudo equatorial (*trans* to P) hydride ligands, as suggested by the low-temperature NMR study. A second minimum (**3b**), located 3.3 kcal mol^{-1} higher, also features a classical dihydride structure. This geometry has C_s symmetry, with the two hydride ligands and two PMe_3 ligands being symmetry related, while the third PMe_3 ligands sits on the mirror plane. The third minimum is a dihydrogen complex with a four-legged piano stool geometry (**3c**), at much higher energy (13 kcal mol^{-1}). Four transition states (TS) interconnecting these minima could be located. As shown in Figure 10, the lowest energy TS is that leading from the global minimum to the symmetric classical isomer, **TS-3a/b**. This rearrangements makes the two H ligands equivalent and at the same time two previously inequivalent P atoms (one trans to the equatorial H atoms and the other one trans to the third P atom) become equivalent. Continuation of this process along the opposite and symmetry related direction exchanges the two H ligands and another pair of P ligands. Thus, this process is in full agreement with the experimental observation of the same activation parameters for the H and P exchange processes. A second exchange mechanism involving the migration of the equatorial hydride to the axial position, thus pushing the axial hydride to the opposite side of the equatorial plane (**TS-3a/a**), is energetically disfavored compared to the previous one. An additional exchange mechanism, whereby the two H ligands exchange their position via rotation of the H_2 ligand in a nonclassical isomer, is also not operative in this case whereas it is rather common for dihydride compounds.[53, 54] Not only is the corresponding transition state (**TS-3a/c**) located higher in energy, this mechanism is also excluded because it would not lead to the simultaneous exchange of the P nuclei. This

observation emphasizes the strong preference of the classical dihydride structure by this complex.

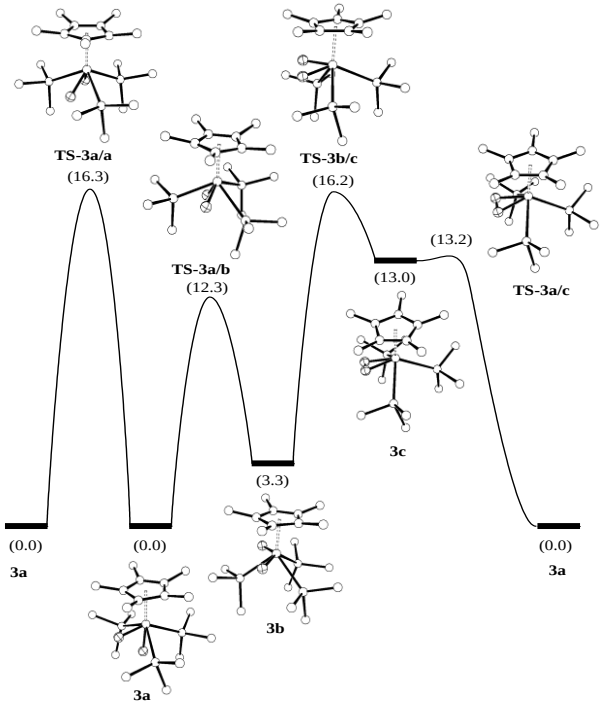

Figure 10. Energies (in kcal mol^{-1}) and geometries of optimized minima and transition states for system $[Cp^*Mo(PMe_3)_3H_2]^+$.

Conclusions

By playing on the ligand electron donating properties and steric bulk, we have managed to produce a thermally stable paramagnetic hydride complex of Mo^{III}, $[Cp^*Mo(PMe_3)_3H]^+$. The steric encumbrance of the coordination sphere, in combination with a relatively important effect of the Cp* ring conformation on the Mo-H bond, has allowed the first experimental observation of Cp* distinct rotamers by the IR investigation of a metal-hydrogen stretching vibration. The same phenomenon occurs for the Mo-H stretching vibration of compound **2** and its neutral precursor **1**. Thus, these compounds exhibit dynamic behavior on very different timescale: restricted rotation around the Mo-Cp* axis with barriers in the range of 1 kcal mol^{-1} (picosecond timescale) and hydride ligand mobility with a barrier of 11.7 kcal

mol^{-1} (millisecond timescale) for compound **1**. The ligand mobility in compound **2** cannot be probed experimentally, because of the broadness of the EPR resonance.

Experimental section

General. All preparations and manipulations were carried out with rigorous exclusion of oxygen and moisture using Schlenk-tube techniques. Solvents were dried by conventional methods and distilled under argon prior to use. The starting material $Cp^*Mo(PMe_3)_3H$ (**1**) was prepared by the published method.[21]

Room temperature (293K) NMR investigations were carried out on a Bruker DPX300 and a Bruker AV300LiQ spectrometers operating at 300.1 MHz (^1H), 121.49 MHz ($^{31}P\{^1H\}$) and 75.47 MHz ($^{13}C\{^1H\}$). Low-temperature ^1H and ^{31}P data were collected with a Bruker AV500 spectrometer, operating at 500.3 MHz and 202.5 MHz, respectively. The temperature was calibrated using a methanol chemical shift thermometer; the accuracy and stability was ±1 K. All samples were allowed to equilibrate at every temperature for at least 3 min. The spectra were calibrated with the residual solvent resonance relative to TMS (^1H, ^{13}C), and with external 85% H_3PO_4 (^{31}P). The conventional inversion-recovery-pulse method (180-τ-90) was used to determine the variable-temperature longitudinal relaxation time T_1, the calculations being done with standard Bruker software. Coupling constants, *J*, are given in hertz. All NMR simulations were performed with SpinWorks software. VT-EPR spectra were measured on a Elexsys E500 BRUKER spectrometer (X-band) equipped with both a frequencemeter and gaussmeter. Cyclic voltammograms were recorded with an EG&G362 potentiostat connected to a Macintosh computer through MacLab hardware/sofware. The electrochemical cell was fitted with an Ag/AgCl reference electrode, a 1 mm-diameter Pt-disk working electrode, and a platinum-wire counter electrode. $[Bu_4N]PF_6$ (*ca.* 0.15 M) was used as the supporting electrolyte. All potentials are reported relative to the ferrocene/ferrocenium

couple. Ferrocene was added and measured as an internal standard at the end of each experiment. The solution IR measurements were performed on ‘‘Infralum 801’’ and “Specord M-82” FT-IR spectrometers. Solid state spectra were measured with a Perkin-Elmer Spectrum 100 FTIR spectrometer (2 cm^{-1} resolution) on the neat solid sample which was pressed inside a quarz crystal. Solution spectra were measured using CaF_2 cells of 0.04–0.22 cm path length. All variable temperature IR measurements in the 190–350 K temperature range were carried out by use of a home-modified cryostat (Carl Zeiss Jena). The cryostat modification allows operating under an inert atmosphere and transferring the reagents (premixed either at low or room temperature) directly into the cell which is pre-cooled or warmed to the required temperature. The accuracy of the temperature adjustment was ±1 K.

Preparation of $[Cp^*Mo(PMe_3)_3H]PF_6$ (2): A suspension of $[Cp_2Fe]PF_6$ (60 mg, 0.18 mmol) in tetrahydrofuran (4 mL) was added drop by drop over a cold solution (193 K) of $Cp^*Mo(PMe_3)_3H$ (88 mg, 0.19 mmol) in tetrahydrofuran (4 mL). The solution color gradually changed from green to dark blue and finally to orange in a few minutes. The reaction mixture was warmed up to 253 K and then it was concentrated to *ca.* 1 mL. Addition of cold diethyl ether (253 K, 8 mL) caused an orange precipitate, which was decanted, washed with cold diethyl ether (253 K, 10 and 8 mL) and vacuum-dried. An orange solid was obtained. Yield: 94 mg (81 %). Anal. Calcd. for $C_{19}H_{37}F_6MoP_4$: C, 37.70; H, 7.16. Found: C, 38.01; H, 6.85. EPR (X-band, THF): g = 2.014 (ΔH_{peak} = 22 G) at 110 K; g = 2.011 (ΔH_{peak} = 180 G) at 253 K. Cyclic voltammetry (THF): $E_{1/2}$ = -0.76 V (ΔE_p = 123 mV) [ferrocene: $E_{1/2}$ = +0.59 V (ΔE_p = 318 mV)]. Cyclic voltammetry (MeCN): $E_{1/2}$ = -0.99 V (ΔE_p = 64 mV) [ferrocene: $E_{1/2}$ = +0.41 V (ΔE_p = 67 mV)].

Preparation of $[Cp^*Mo(PMe_3)_3H_2]BF_4$ (3): HBF_4 (50% w/w in diethyl ether, 30 μL, 0.20 mmol) was added to a cold solution (273 K) of $Cp^*Mo(PMe_3)_3H$ (89 mg, 0.19 mmol) in diethyl ether (8 mL). Immediate formation of a whitish solid was monitored. The suspension was left to stir for 10 min and then it was decanted. The resulting solid was washed with

diethyl ether (3 x 10 mL) and dried *in vacuo*. A white solid was obtained. Yield: 96 mg (82 %). Anal. Calcd. for $C_{19}H_{44}BF_4MoP_3$: C, 41.63; H, 8.09. Found: C, 41.41; H, 7.94. $^{31}P\{^1H\}$ NMR ($CDCl_3$): δ 4.7 (s). ^1H NMR ($CDCl_3$): δ -4.52 (q, *J* = 49.0 Hz, 2 H, Mo-H), 1.55 (pseudo q, *J* = 2.6 Hz, 27 H, $P(CH_3)_3$), 1.96 (s, 15 H, $C_5(CH_3)_5$). ^1H NMR (500.3 MHz, CD_2Cl_2, 200K): δ -6.53 (vt, 1H, 50Hz), -3.03 (vdq, 1H), 1.42 (s, 9H, PMe_3), 1.47 (s, 18H, PMe_3), 1.88 (s, 15H, Cp*). $^{31}P\{^1H\}$ (203.5 MHz, CD_2Cl_2, 200K): δ -1.2 (t, 1P, J = 23 Hz), 7.6 (d, 1P, J = 23Hz). The compound slowly decomposes in $CDCl_3$ and CD_2Cl_2 at 290K.

NMR and EPR tube monitoring experiments. For all NMR and EPR tube experiments, the sample (ca. 10 mg) was charged as a solid in the glovebox under argon and the tube was sealed with a rubber septum and further wrapped with parafilm. The solvents and/or other solutions were added to the NMR tube by cannula transfer on a Schlenk line. All solvents were degassed by three freeze-pump-thaw cycles prior to use.

Computational details.

Quantum mechanical calculations were performed with the Gaussian03 package[55] at the DFT/B3LYP level.[56-58] Core electrons of the Mo and P atoms were described using the effective core pseudopotentials of Hay-Wadt[59, 60] and valence electrons were described with the standard LANL2DZ basis set.[55] In the case of the P atoms, a set of d type functions was added.[61] Carbon and hydrogen atoms non-bonded to the metal were described with a 6-31G basis set, carbon atoms linked to the metal were described with a 6-31g* basis set, and the hydride hydrogen atom was described with a 6-31g** basis set.[62-71] All minima and transition states were characterized by analytically computing the Hessian matrix and no scaling factors were used for frequencies. Information on atom coordinates (xyz files) for all optimized structures is collected in the supplementary material.

X-ray Structure Determination. A single crystal of $[Cp^*Mo(PMe_3)_3H]PF_6$ was mounted under inert perfluoropolyether at the tip of glass fibre and cooled in the cryostream of an Oxford-Diffraction XCALIBUR CCD diffractometer and data were collected using the

monochromatic MoKα radiation (λ= 0.71073). The structure was solved by direct methods (SIR97)[72] and refined by least-squares procedures on F^2 using SHELXL-97.[73] All H atoms attached to carbon were introduced in calculation in idealised positions and treated as riding models. The hydride H atom was located in difference Fourier syntheses and was freely refined with isotropic thermal parameter. The drawing of the molecule was realised with the help of ORTEP32.[74] Crystal data and refinement parameters are shown in Table 2. Crystallographic data (excluding structure factors) have been deposited with the Cambridge Crystallographic Data Centre as supplementary publication no. CCDC 603848. Copies of the data can be obtained free of charge on application to the Director, CCDC, 12 Union Road, Cambridge CB2 1EZ, UK (fax: (+44) 1223-336-033; e-mail: deposit@ccdc.cam.ac.uk).

Table 2. Crystal data and structure refinement for $[Cp^*Mo(PMe_3)_3]PF_6$.

Empirical formula	$C_{19}\ H_{43}\ F_6\ Mo\ P_4$	
Formula weight	605.35	
Temperature	180(2) K	
Wavelength	0.70930 Å	
Crystal system	Monoclinic	
Space group	P 2_1/n	
Unit cell dimensions	a = 9.9347(11) Å	α= 90.0°
	b = 15.5051(15) Å	β= 90.827(9)°
	c = 17.4655(19) Å	γ = 90.0°
Volume	2690.1(5) Å3	
Z	4	
Density (calculated)	1.495 Mg/m^3	
Absorption coefficient	0.772 mm^{-1}	
F(000)	1252	
Crystal size	0.25 x 0.102 x 0.071 mm^3	
Theta range for data collection	3.08 to 24.97°.	
Index ranges	-9 ≤h ≤11, -18 ≤k ≤18, -20 ≤l ≤20	
Reflections collected	18043	
Independent reflections	4734 [R(int) = 0.0944]	
Completeness to theta = 24.97°	99.8 %	
Absorption correction	Semi-empirical from equivalents	

Max. and min. transmission	0.9769 and 0.8497
Refinement method	Full-matrix least-squares on F^2
Data / restraints / parameters	4734 / 0 / 290
Goodness-of-fit on F^2	0.932
Final R indices [I>2sigma(I)]	R1 = 0.0508, wR2 = 0.1097
R indices (all data)	R1 = 0.0779, wR2 = 0.1243
Largest diff. peak and hole	0.796 and -0.887 e.$Å^{-3}$

Acknowledgement

We thank bilateral grants (PICS and GDRE "CH2D", France-Russia; LEA, France-Spain) and National support from the Institut Universitaire de France and CNRS (France), the RFBR (08-03-00464) and the Division of Chemistry and Material Sciences of RAS (Russia) and the Spanish MEC (Project CTQ2005-09000-C02-01 and Consolider Ingenio 2010 CDS2007-00006). MB thanks the Spanish Ministerio de Educación y Ciencia for a post-doctoral fellowship and the Spanish MEC/Universidad de Zaragoza for funding through the "Ramón y Cajal" program.

References

1 Ryan, O. B.; Tilset, M.; Parker, V. D., *J. Am. Chem. Soc.* **1990,** 112, 2618-2626.
2 Smith, K.-T.; Rømming, C.; Tilset, M., *J. Am. Chem. Soc.* **1993,** 115, 8681-8689.
3 Pleune, B.; Morales, D.; Meunier-Prest, R.; Richard, P.; Collange, E.; Fettinger, J. C.; Poli, R., *J. Am. Chem. Soc.* **1999,** 121, 2209-2225.
4 Poli, R., *Paramagnetic mono- and polyhydrides of the transition metals*. In *Recent Advances in Hydride Chemistry*, Poli, R.; Peruzzini, M., Eds., Elsevier Science: Amsterdam, 2001; 'Vol.' pp 139-188.
5 Foerster, S.; Stein, M.; Brecht, M.; Ogata, H.; Higuchi, Y.; Lubitz, W., *J. Am. Chem. Soc.* **2003,** 125, 83-93.
6 Igarashi, R. Y.; Laryukhin, M.; Dos Santos, P. C.; Lee, H.-I.; Dean, D. R.; Seefeldt, L. C.; Hoffman, B. M., *J. Am. Chem. Soc.* **2005,** 127, 6231-6241.
7 Gloaguen, F.; Lawrence, J. D.; Rauchfuss, T. B., *J. Am. Chem. Soc.* **2001,** 123, 9476-9477.
8 Mejia-Rodriguez, R.; Chong, D. S.; Reibenspies, J. H.; Soriaga, M. P.; Darensbourg, M. Y., *J. Am. Chem. Soc.* **2004,** 126, 12004-12014.
9 Kristjánsdóttir, S. S.; Norton, J. R., *Acidity of Hydrido Transition Metal Complexes in Solution*. In *Transition Metal Hydrides*, Dedieu, A., Eds., VCH: New York, 1992; 'Vol.' pp 309-359.
10 Jacobsen, H.; Berke, H., *Hydridicity of Transition Metal Hydrides and its Implications for Reactivity*. In *Recent Advances in Hydride Chemistry*, Poli, R.; Peruzzini, M., Eds., Elsevier Science: Amsterdam, 2001; 'Vol.' pp 89-116.

[11] Baya, M.; Houghton, J.; Daran, J.-C.; Poli, R., *Angew. Chem., Int. Ed. Engl.* **2007,** 46, 429-432.
[12] Baya, M.; Houghton, J.; Daran, J.-C.; Poli, R.; Male, L.; Albinati, A.; Guttman, M., *Chem. Eur. J.* **2007,** 13, 5347-5359.
[13] Fettinger, J. C.; Kraatz, H.-B.; Poli, R.; Quadrelli, E. A.; Torralba, R. C., *Organometallics* **1998,** 17, 5767-5775.
[14] Abugideiri, F.; Kelland, M. A.; Poli, R.; Rheingold, A. L., *Organometallics* **1992,** 11, 1303-1311.
[15] Connelly, N. G.; Geiger, W. E., *Chem. Rev.* **1996,** 96, 877-910.
[16] Schultz, A. J.; Stearley, K. L.; Williams, J. M.; Mink, R.; Stucky, G. D., *Inorg. Chem.* **1977,** 16, 3303-6.
[17] Tsai, Y.-C.; Johnson, M. J. A.; Mindiola, D. J.; Cummins, C. C., *J. Am. Chem. Soc.* **1999,** 121, 10426-10427.
[18] Brammer, L.; Zhao, D.; Bullock, R. M.; Mcmullan, R. K., *Inorg. Chem.* **1993,** 32, 4819-4824.
[19] Abugideiri, F.; Fettinger, J. C.; Keogh, D. W.; Poli, R., *Organometallics* **1996,** 15, 4407-4416.
[20] Jiménez-Tenorio, M.; Puerta, M. C.; Valerga, P., *Organometallics* **1994,** 13, 3330-3337.
[21] Shin, J. H.; Parkin, G., *Polyhedron* **1994,** 13, 1489-1493.
[22] Marat, K., *SpinWorks Version 2.5.4*. ed.; 2006.
[23] Kalck, P.; Poilblanc, R., *J. Organometal. Chem.* **1969,** 19, 115-121.
[24] Faller, J. W.; Anderson, A. S., *J. Am. Chem. Soc.* **1970,** 92, 5852-5860.
[25] Cheng, T. Y.; Brunschwig, B. S.; Bullock, R. M., *J. Am. Chem. Soc.* **1998,** 120, 13121-13137.
[26] Baya, M.; Crochet, P.; Esteruelas, M. A.; Gutiérrez-Puebla, E.; Ruiz, N., *Organometallics* **1999,** 18, 5034-5043.
[27] Du Plooy, K. E.; Moll, U.; Wocadlo, S.; Massa, W.; Okuda, J., *Organometallics* **1995,** 14, 3129-3131.
[28] Liu, A. H.; Murray, R. C.; Dewan, J. C.; Santarsiero, B. D.; Schrock, R. R., *J. Am. Chem. Soc.* **1987,** 109, 4282-4291.
[29] Smith, J. M.; Coville, N. J., *Organometallics* **1996,** 15, 3388-3392.
[30] Poli, R., *Organometallics* **1990,** 9, 1892-1900.
[31] Lin, Z.; Hall, M. B., *Organometallics* **1993,** 12, 19-23.
[32] Baya, M.; Maresca, O.; Poli, R.; Coppel, Y.; Maseras, F.; Lledós, A.; Belkova, N. V.; Dub, P. A.; Epstein, L. M.; Shubina, E. S., *Inorg. Chem.* **2006,** 45, 10248-10262.
[33] Ittel, S. D.; Krusic, P. J.; Meakin, P., *J. Am. Chem. Soc.* **1978,** 100, 3264-3266.
[34] Krusic, P. J., *J. Am. Chem. Soc.* **1981,** 103, 2131-2133.
[35] Mao, F.; Sur, S. K.; Tyler, D. R., *J. Am. Chem. Soc.* **1989,** 111, 7627-7628.
[36] Macphail, R. A.; Strauss, H. L., *J. Chem. Phys.* **1985,** 82, 1156-1166.
[37] Wood, K. A.; Strauss, H. L., *J. Phys. Chem.* **1990,** 94, 5677-5684.
[38] Turner, J. J.; Gordon, C. M.; Howdle, S. M., *J. Phys. Chem.* **1995,** 99, 17532-17538.
[39] Grevels, F. W.; Kerpen, K.; Klotzbucher, W. E.; Mcclung, R. E. D.; Russell, G.; Viotte, M.; Schaffner, K., *J. Am. Chem. Soc.* **1998,** 120, 10423-10433.
[40] Londergan, C. H.; Kubiak, C. P., *Chem.--Eur. J.* **2003,** 9, 5962-5969.
[41] Cahoon, J. F.; Sawyer, K. R.; Schlegel, J. P.; Harris, C. B., *Science* **2008,** 319, 1820-1823.
[42] Belkova, N. V.; Revin, P. O.; Epstein, L. M.; Vorontsov, E. V.; Bakhmutov, V. I.; Shubina, E. S.; Collange, E.; Poli, R., *J. Am. Chem. Soc.* **2003,** 125, 11106-11115.
[43] Belkova, N. V.; Dub, P. A.; Baya, M.; Houghton, J., *Inorg. Chim. Acta* **2007,** 360, 149–162.

[44] Dub, P. A.; Belkova, N. V.; Lyssenko, K. A.; Silantyev, G. A.; Epstein, L. M.; Shubina, E. S.; Daran, J.-C.; Poli, R., *Organometallics* **in press**.
[45] Poli, R., *J. Organometal. Chem* **2004,** 689, 4291–4304.
[46] Salomon, O.; Reiher, M.; Hess, B. A., *J. Chem. Phys.* **2002,** 117, 4729-4737.
[47] Harvey, J.; Aschi, M., *Faraday Disc.* **2003,** 124, 129-143.
[48] Poli, R.; Harvey, J. N., *Chem. Soc. Rev.* **2003,** 32, 1-8.
[49] Wasbotten, I. H.; Ghosh, A., *Inorg. Chem.* **2007,** 46, 7890-7898.
[50] Conradie, J.; Ghosh, A., *J. Chem. Theory Comput.* **2007,** 3, 689-702.
[51] Bullock, R. M.; Song, J.-S.; Szalda, D. J., *Organometallics* **1996,** 15, 2504-2516.
[52] Cheng, T.-Y.; Szalda, D. J.; Zhang, J.; Bullock, R. M., *Inorg. Chem.* **2006,** 45, 4712-4720.
[53] Gusev, D. G.; Berke, H., *Chem. Ber.* **1996,** 129, 1143-1155.
[54] Kubas, G. J., *J. Organomet. Chem.* **2001,** 635, 37-68.
[55] Frisch, M. J., *et al.*, *Gaussian 03, Revision C.02*. ed.; Gaussian, Inc.: Wallingford CT, 2004.
[56] Becke, A. D., *J. Chem. Phys.* **1993,** 98, 5648-5652.
[57] Perdew, J. P., *Electronic Structure of Solids*. In Ziesche, P.; Eschrig, H., Eds., Akademie Verlag: Berlin, 1991; 'Vol.' pp 11.
[58] Perdew, J. P.; Wang, Y., *Phys. Rev. B* **1992,** 45, 13244-13249.
[59] Wadt, W. R.; Hay, P. J., *J. Chem. Phys.* **1985,** 82, 284-298.
[60] Hay, P. J.; Wadt, W. R., *J. Chem. Phys.* **1985,** 82, 299-310.
[61] Höllwarth, A.; Bohme, M.; Dapprich, S.; Ehlers, A.; Gobbi, A.; Jonas, V.; Kohler, K.; Stegmann, R.; Veldkamp, A.; Frenking, G., *Chem. Phys. Lett.* **1993,** 208, 237-40.
[62] Ditchfield, R.; Hehre, W. J.; Pople, J. A., *J. Chem. Phys.* **1971,** 54, 724-8.
[63] Hehre, W.; Ditchfie, R.; Pople, J., *J. Chem. Phys.* **1972,** 56, 2257-2261.
[64] Hariharan, P. C.; Pople, J. A., *Mol. Phys.* **1974,** 27, 209-14.
[65] Gordon, M. S., *Chem. Phys. Lett.* **1980,** 76, 163-8.
[66] Hariharanan, P.; Pople, J. A., *Theor. Chim. Acta* **1973,** 28, 213-222.
[67] Blaudeau, J. P.; Mcgrath, M. P.; Curtiss, L. A.; Radom, L., *J. Chem. Phys.* **1997,** 107, 5016-5021.
[68] Francl, M. M.; Pietro, W. J.; Hehre, W. J.; Binkley, J. S.; Gordon, M. S.; Defrees, D. J.; Pople, J. A., *J. Chem. Phys.* **1982,** 77, 3654-3665.
[69] Binning, R. C.; Curtiss, L. A., *J. Comput. Chem.* **1990,** 11, 1206-1216.
[70] Rassolov, V. A.; Pople, J. A.; Ratner, M. A.; Windus, T. L., *J. Chem. Phys.* **1998,** 109, 1223-1229.
[71] Rassolov, V. A.; Ratner, M. A.; Pople, J. A.; Redfern, P. C.; Curtiss, L. A., *J. Comput. Chem.* **2001,** 22, 976-984.
[72] Altomare, A.; Burla, M.; Camalli, M.; Cascarano, G.; Giacovazzo, C.; Guagliardi, A.; Moliterni, A.; Polidori, G.; Spagna, R., *J. Appl. Cryst.* **1999,** 32, 115-119.
[73] Sheldrick, G. M., *SHELXL97. Program for Crystal Structure refinement*. ed.; University of Göttingen: Göttingen, Germany, 1997.
[74] Farrugia, L. J., *J. Appl. Crystallogr.* **1997,** 32, 565.

TOC Graphic

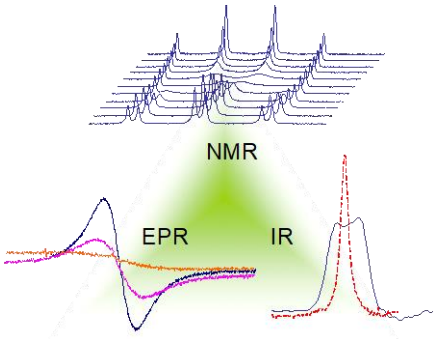

TOC text

The pair of redox-related complexes $[Cp^*Mo(PMe_3)_3H]^{n+}$ (n = 0, 1) show exchange of the phosphine positions (in the ms timescale for n = 0, frozen at low temperature by NMR; not resolved for n = 1) and Cp* ligand rotation (in the ps timescale, frozen in the solution IR spectrum for both complexes).